Title
SPIN-FORBIDDEN RADIATIVE DECAY OF THE STATE OF O2+

Author
Bustamente, S.W.

Publication Date
1986-08-01

LBL-22097 c.2
Preprint

Lawrence Berkeley Laboratory
UNIVERSITY OF CALIFORNIA

Materials & Molecular
Research Division

Submitted to Journal of Chemical Physics

SPIN-FORBIDDEN RADIATIVE DECAY OF THE $\alpha\,^4\Pi_u$ STATE OF O_2^+

S.W. Bustamente, M. Okumura, D. Gehrlich,
H.S. Kwok, L.R. Carlson, and Y.T. Lee

August 1986

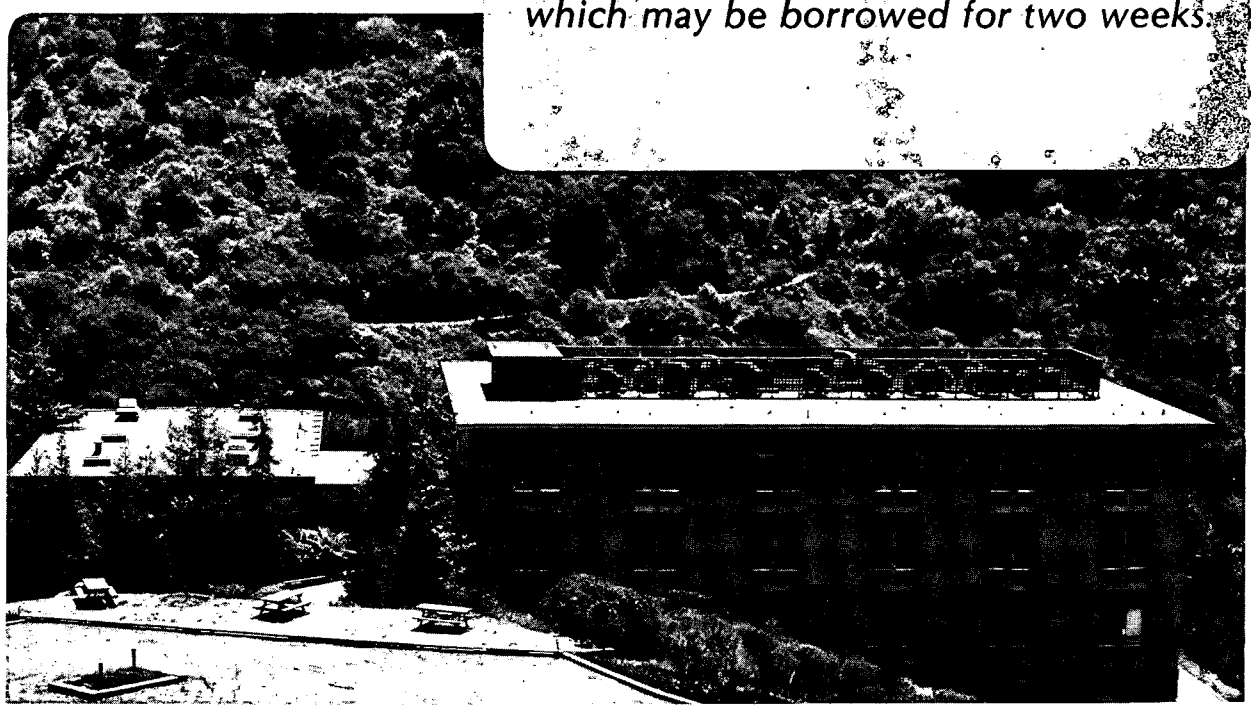

Prepared for the U.S. Department of Energy under Contract DE-AC03-76SF00098

DISCLAIMER

Spin-Forbidden Radiative Decay of the $a^4\Pi_u$ State of O_2^+

S. W. Bustamente,[a] M. Okumura, D. Gehrlich,[b] H. S. Kwok,[c]

L. R. Carlson,[d] and Y. T. Lee

Materials and Molecular Research Division, Lawrence Berkeley Laboratory and Department of Chemistry, University of California, Berkeley, CA 94720 USA

ABSTRACT

The spin-forbidden radiative decay of $a^4\Pi_u$ O_2^+ has been measured in a radio frequency octopole ion trap. Photodissociation is used to probe the $a^4\Pi_u$ population as a function of trapping time. We have found that the $a^4\Pi_u$ state exhibits a multiple exponential decay, ranging from a few milliseconds to hundreds of milliseconds. The state dependence of the decay is seen in the photodissociation spectrum ($b^4\Sigma_g^- \leftarrow a^4\Pi_u$), which changes dramatically from 0.1 ms to 100 ms. The major changes in the spectrum are simulated by assuming that the F_2 and F_3 spin components of the $a^4\Pi_u$ state decay faster than the F_1 and F_4 components. We can account for this dependence on spin sub-level by assuming that the primary mechanism for radiative decay arises from spin-orbit coupling of the $a^4\Pi_u$ and $A^2\Pi_u$ states. Our results suggest that the $a^4\Pi_u$ radiative lifetime of 0.22 s measured by O'Keefe and McDonald reflects the decay of only the longest living $a^4\Pi_u$ sub-levels.

---

[a]Current address: Hughes Aircraft Corporation, P.O. Box 2999, Torrance, CA 90509.

[b]Permanent address:Dept. of Physics, Universitat Freiburg, D–7800 Freiburg, West Germany.

[c]Current address:Dept. of Physics, State University of New York, Buffalo NY.

[d]Current address:Spectra Physics, Mountain View, CA

I. INTRODUCTION

In the E- and F-regions of the ionosphere, O_2^+ is a primary ion created by the solar photoionization of oxygen.[1] Closer to Earth, in the D-region, reactions of O_2^+ are the first steps in many chemical schemes.[2] In these regions, as well as in discharges, auroras, and other gaseous plasmas, the metastable $a^4\Pi_u$ state of O_2^+ plays an important role in oxygen ion chemistry. This state, lying 4 eV above the $X^2\Pi_g$ ground state,[3] is the lowest state in the quartet manifold. It is often created with a significant population by photoionization, Penning ionization, and electron bombardment, after higher electronic states have cascaded down. Many reactions are endothermic for the ground state but exothermic for the metastable state, and the $a^4\Pi_u$ state is generally more reactive than the $X^2\Pi_g$ ground state.[4]

Spectra in the visible glow near the cathode of an oxygen discharge were identified early on as emission within the quartet manifold to the $a^4\Pi_u$ state of O_2^+. Several high resolution studies of the fluorescence spectrum in the visible, the First Negative Band, were done[5] and the spectrum was assigned as the $b^4\Sigma_g^- \rightarrow a^4\Pi_u$ transition. The relevant potential energy curves are illustrated in Fig. 1. In 1975, Vestal, Mauclaire, and Futrell[6] observed the photodissociation of O_2^+ with 6000 Å light. Because the ground state dissociation energy is 6.8 eV(1830 Å), it was assigned as photodissociation of the metastable $a^4\Pi_u$ state. Moseley *et al.*[7] were the first to resolve structure in the photodissociation spectrum. Their work and subsequent experiments have shown that the photodissociation spectrum consists of a discrete spectrum arising from transitions to predissociating states(transitions labeled I in Fig. 1) and a broad continuum of transitions to repulsive states(labeled II in Fig. 1). Carrington, Roberts, and Sarre obtained very high resolution spectra[8] using fast ion beam laser absorption spectroscopy, in which absorption to predissoci-

ating states were observed by detecting the O^+ products. They correctly attributed the discrete photodissociation spectrum to transitions of the First Negative Band, from the metastable $a^4\Pi_u$ state to predissociating levels of the $b^4\Sigma_g^-$ state. Several researchers, most notably the group at SRI, have exploited the reduced Doppler width and high sensitivity of the fast ion beam photofragment spectroscopy to obtain extensive ultrahigh resolution spectra. By merging the photodissociation and fluorescence data, Hansen, Cosby, and Moseley[9] have made the most detailed analysis of any quartet-quartet transition; the visible spectroscopy of the $a^4\Pi_u$ state is therefore well understood.[10,11]

Because it decays by a spin-forbidden transition to the ground $X^2\Pi_g$ state, the $a^4\Pi_u$ state is long-lived. Knowledge of the lifetime of such a reactive, metastable species is clearly desirable. Based on flight times, Vance[12] has estimated a lower bound for the radiative lifetime of 1 ms, too long to be readily measured by conventional techniques. In this paper, we describe an ion trapping and photodissociation experiment with which we have observed the radiative decay of metastable $a^4\Pi_u$ O_2^+. The machine has a high vacuum, radio frequency(rf) octopole ion trap, which enables us to trap the ions without collisions or perturbations for times as long as one second. The O_2^+ ions are formed by electron impact ionization, creating a substantial population in the $a^4\Pi_u$ state. Visible light photodissociates the metastable state, but is not energetic enough to dissociate the ground state. Thus, visible photodissociation to $O^+ + O$ can be used to selectively detect the metastable state population. The experiment is performed by trapping the ions and, after a variable delay, photodissociating the ions to measure the fraction remaining in the $a^4\Pi_u$ state. We can observe the decay of this state by measuring the O^+ photofragment count as a function of trapping time. Furthermore, the low resolution photodisso-

ciation spectra, scanned at different trapping times, allows us to examine the state dependence of the $a^4\Pi_u$ radiative decay.

Since the completion of this work, O'Keefe and McDonald[13] have reported measurements of the radiative decay of both the $a^4\Pi_u$ state of O_2^+ and the $a^3\Sigma^+$ state of NO^+ using an ion cyclotron resonance (ICR) trap. For O_2^+, they have measured rates of the charge transfer reaction with Ar at pressures of 10^{-7} torr and higher, a reaction which proceeds only for the $a^4\Pi_u$ state, not the $X^2\Pi_g$ state. By extrapolating the observed rates to zero pressure, they have obtained a lifetime of 0.22 s for the $a^4\Pi_u$ state of O_2^+. Our work is consistent with their results, and sheds new light on this spin-forbidden decay.

II. EXPERIMENTAL

The apparatus, shown schematically in Fig. 2, is a tandem mass spectrometer with a radio frequency octopole ion guide between the two mass filters. The ion guide helps to confine very slow ions, with energies less than 1 eV, but can also be used as an ion trap, capable of storing ions for long times. The first mass spectrometer selects only the parent ions for injection into the octopole, where the ions are trapped and then photolyzed. The final mass spectrometer is used to mass-analyze the photodissociation products. The experiment is thus similar in concept to ion photodissociation experiments using ICR traps. With a time resolution of approximately 1 ms and trap region pressures of less than 10^{-9} torr, the apparatus is well suited for measuring vibrational and forbidden decays.

A. The Radio Frequency Octopole Ion Trap

Ion traps have been used successfully to measure the lifetimes of a number of excited states of ions. For atomic ions, several forbidden transition lifetimes have been measured. The 58.6 ± 12.9 s lifetime of 2^3S_1 Li^+, the 47 ± 16 s lifetime of $^5D_{5/2}$ Ba^+, the 17.5 ± 4 s lifetime of $^5D_{3/2}$ Ba^+, and the 0.090 ± 0.015 s lifetime of $^2D_{5/2}$ Hg^+ have been measured in ion traps by optical pumping schemes.[14] Knight has measured a 4.2 ± 0.6 ms lifetime for metastable $^5S_2$ N^+ by directly observing the decay of the spontaneous emission.[15] Several workers have used rf quadrupole[16] and ICR traps[17] to determine allowed radiative lifetimes and collisional deactivation rates for molecular ions using laser induced fluorescence.

The confinement of ions in three dimensional radio frequency quadrupole (Paul) traps is well established. Because the equation of motion of ions can be solved analytically, the properties of quadrupole traps are well understood.[18,19] Trapping properties are not however limited to quadrupole fields. In an oscillating, spatially inhomogeneous electric field the trajectory of a slowly moving ion can be separated into a fast, small amplitude oscillation (the micromotion) and a slower time-averaged motion,[18,20] provided the frequency of oscillation is fast relative to the ion velocity. The micromotion creates an adiabatic effective potential for the time-averaged motion.

Teloy and Gehrlich have pioneered the use of inhomogeneous rf fields for confining, guiding and trapping ions.[21,22] For an ideal rf electric multipole field with $2n$ poles, the effective potential is given by

$$U_{\text{eff}}(r) = n^2 K \left(\frac{r}{r_0}\right)^{2n-2} \tag{1}$$

where

$$K = \frac{q^2 V_0^2}{m\omega^2 r_0{}^2} \tag{2}$$

for a particle of charge q and mass m inside a multipole of radius r_0. The voltage of the rf is V_0, the frequency ω. For a dipole field, $n = 1$, for a quadrupole $n = 2$, and for an octopole field $n = 4$. These trapping potentials are valid within certain limits, which are discussed in detail by Teloy and Gehrlich.

The rf octopole was primarily developed to guide low energy ions in experiments measuring integral cross sections of ion-molecule reactions.[21,22,23] For a rf octopole field, the effective potential varies as $(r/r_0)^6$ while for a quadrupole field, it varies as $(r/r_0)^2$. Ions in the center of an octopole trap are thus less perturbed by the oscillating fields. Furthermore, the octopole trapping well is four times deeper than the quadrupole well at the same frequency, voltage, and mass. Thus, the octopole potential is flatter in the center and has steeper walls than the quadrupole effective potential. The depth of the trap also depends inversely on the mass; therefore, fragments created in the trap by photodissociation will experience a deeper potential well than their heavier parent ions. Further details can be found in discussions by Teloy and Gehrlich[21,22], and by Ervin and Armentrout.[23]

The octopole guide is made of eight parallel molybdenum rods, 500 cm long, 0.32 cm in diameter, equally spaced on a 1.25 cm diameter circle. Molybdenum is used to minimize surface charge, which would adversely affect low energy ions. Alternate rods of the octopole are at opposite phases. The leads are connected to a coil, and the octopole acts as the capacitor in the resulting resonant LC circuit. The circuit is driven inductively by a small rf power supply. The rf frequency is 14 MHz, with an amplitude of ~250 V. The rods are thicker than those used by Ervin and Armentrout.[23] As a result, the field probably deviates more from a pure

hyperbolic octopole field, but the trapping volume is shielded more effectively from potentials outside the trap.

The radio-frequency traps the ions radially, transverse to the axis of the ion octopole. The ions are confined inside the trap by raising the dc potential of the entrance and exit lens elements at either end of the rods. These lenses protrude into the trap, to minimize problems while trapping with rf fringe fields at the ends of the trap. The ions would thus bounce back and forth between these elements. To trap the ions, the potential of the lens was typically 10 V above the dc bias of the rods. When trapped, the average energy of the O_2^+ ions was about 0.65 eV.

For the quadrupole rf field, Dawson has shown that only certain initial ion trajectories found within an acceptance ellipse in phase space will be trapped.[24] Those with initial momenta or spatial position outside the acceptance ellipse are unstable and will be ejected. Similar conditions are imposed on the initial ion trajectories for the octopole trap. Approximately 50% of the parent O_2^+ ions are lost in the first 50 ms; however, the remaining ions are efficiently trapped. No additional loss of O_2^+ has been observed for trapping times as long as 5 s. Fig. 3 shows the decay of O_2^+ in the first 100 ms.

B. Experimental Details

Fig. 2 is a schematic drawing of the machine. Ions were produced by electron impact ionization of oxygen. O_2^+ ions were selected by a sector magnet mass filter, deflected 90°, and then pulsed into the ion trap. After a selected delay time, a pulsed dye laser was fired into the trap to dissociate the ions in the metastable state. The ions were released from the trap through the exit lens element. O^+ products were selected by a final quadrupole mass filter, and then counted by the

ion detection system. The radio frequency to the trap was turned off for 5 ms to ensure that the ion trap was free of ions at the start of the next data cycle. The sequence was repeated—without the laser firing—to measure the background O^+ counts.

Spectra were taken by scanning the wavelength of a pulsed tunable dye laser while keeping the trapping time fixed. The dye laser was tuned in the visible, in the region of the First Negative Band ($b^4\Sigma_g^- \leftarrow a^4\Pi_u$). Fig. 4 shows a typical wavelength scan at two trapping times. The observed resolution was about 1 cm^{-1}.

Lifetimes were measured at fixed laser wavelengths by incrementing the trapping time. Fig. 3 shows the decay of O^+ photoproduct yield as a function of trapping time for the indicated wavelengths. As stated above, the parent O_2^+ population in the trap, with the laser off, decreased by approximately 50% in the first 50 ms. All O^+ decay curves were therefore normalized to compensate for the loss of parent ions; these curves are shown in Fig. 5. At the pressures used in this experiment, collisions were negligible for times less than one second. The loss of O_2^+ was therefore caused primarily by the inefficiency of the ion trap.

The source was a modified Extranuclear Laboratories electron impact ionizer. The O_2^+ ions were created by ionizing 5×10^{-4} torr of oxygen. The electron energy was approximately 80 eV. After a few microseconds, the O_2^+ formed under these conditions should be essentially in two electronic states: 20% to 50% in the $a^4\Pi_u$ state and the remainder in the $X^2\Pi_g$ state.[13,25] The precise value was unimportant, since we measured only relative population changes. The rotational temperature should be close to the initial temperature of 300 K, but many vibrational states were probably populated.

The ions were focused, and then accelerated to 350 eV. The ions passed through

a second differential chamber with ion optics, maintained at approximately 2×10^{-7} torr by a liquid-nitrogen trapped six inch diffusion pump. The O_2^+ ion beam was mass-selected by a 60° sector magnet mass analyzer with a 20 cm radius of curvature. To enhance the resolution and transmission, we used electrostatic quadrupole lens pairs[26] to focus the beam when it entered into and exited from the magnetic field. The analyzer was scanned by tuning the magnetic field; the flight tube was at ground. Resolution was typically $M/\Delta M$=150 or better at an ion energy of 350 eV. Differential pumping kept the pressure in the mass analyzer region at approximately 2×10^{-8} torr.

After leaving the mass analyzer, the ions passed through a small tube which limited conductance between the sector magnet region and the ultrahigh vacuum chamber. The latter region was kept at pressures of approximately 8×10^{-10} torr by a 220 l/s ion pump. An electrostatic quadrupole field deflector, based on the design of Zeman,[27] bent the ion beam by 90° into a path collinear with the laser. This deflector allowed the two beams to merge without introducing apertures which would perturb the field. The poles of the deflector were circular, approximating the hyperbolic equipotential surfaces of a quadrupole field. The fields of the poles were terminated by grounded plates, but there were no shim electrodes to correct for aberrations. The ions were then slowed to about 5 eV by a constant gradient decelerator and focused into the trap, where their final energy was approximately 0.5 eV.

To trap the ions, the voltage of the input lens was kept low for 0.6 ms to focus the ions into the trap, then raised. The ions were kept in the trap for a delay time generated by the LSI-11 computer. The laser was then fired (on alternate cycles). The voltage of the exit lens element was lowered for 4.5 ms to release the ions.

After the ions left the trap, they were focused into a quadrupole mass spectrometer(Extranuclear Laboratories) and then detected using either a Ceratron (muRata Corp.) ceramic electron multiplier or a Daly detector.[28] In this experiment, measurements were made by pulse counting, using the Daly detector only. Data acquisition was controlled by a Digital Equipment Corporation LSI-11 microcomputer interfaced with a Kinetic Systems CAMAC Crate.

The spectrometer was built so that the laser beam could pass completely through the machine without striking any obstructions. The quadrupole mass filter, the octopole ion guide, and the ion optics were all collinear with the laser beam, while the detector components were off-axis. The laser beam entered the vacuum chamber through a sapphire window, down the axis of the ion optics, through the quadrupole deflection field, and out a second window. This design prevented spurious laser-correlated signal from photoelectrons or desorption caused by the laser pulse striking metal surfaces.

The laser was a Quanta Ray PDL-1 pulsed dye laser pumped by a DCR-1A Nd:YAG laser. The linewidth of the laser was ≈ 0.4 cm^{-1}, and the pulse width was ≈ 8 ns. The repetition rate used was 4.2 Hz, the beam diameter 0.4 cm. The laser was carefully aligned so that it passed cleanly through the spectrometer. No laser correlated signal was observed when the ions were not in the interaction region. Fig. 6 shows the O^+ photofragment signal as a function of laser pulse energy at 5320 Å. The lifetime measurements were carried out with pulse energies of ≈ 0.7 mJ, well in the regime of linear power dependence. The best resolution observed in the wavelength scans was about 1 cm^{-1}. The average energy of the trapped ions was approximately 0.65 eV with an estimated spread of about 0.3 eV. After the ions had made several round trips in the trap, the initial axial energy of the ions was

distributed to all degrees of freedom. For O_2^+ at a median energy of 0.65 eV, the Doppler width should be 0.3 cm^{-1} at 5000 Å; convoluted with the 0.4 cm^{-1} laser linewidth, this width was consistent with but narrower than the observed 1 cm^{-1} resolution.

III. RESULTS

Fig. 4 shows the photodissociation spectrum of the $a^4\Pi_u$ state at two times, 0.1 ms and 100 ms, scanned over a region including two band sequences $\Delta v=2$ and $\Delta v=3$. Ionization of O_2 and cascading from higher quartet states should lead to $a^4\Pi_u$ O_2^+ in many vibrationally excited states, although the rotational distribution should remain close to a room temperature Boltzmann distribution. Several vibrational bands thus contribute to each sequence. The initial vibrational and rotational populations will not relax by pure rotational or rovibrational transitions during the time of the experiment. These transitions are dipole-forbidden in homonuclear diatomics and the quadrupole transition moments are very weak.

As can be seen in Fig. 4, there is a noticeable change in the spectrum after the O_2^+ have been trapped for 100 ms, indicating a very strong state dependence of the radiative decay rate of the spin-forbidden transition. To understand the mechanism, we must consider the fine structure splitting of the two states.

For both the $a^4\Pi_u$ and $b^4\Sigma_g^-$ states, the four-fold spin degeneracy is lifted; for a given value of N, the rotational quantum number, there are four fine structure components F_1 through F_4. The $b^4\Sigma_g^-$ state, with no angular momentum projection along the internuclear axis, is described by Hund's case (b). The four components are: F_1 $(J = N+3/2)$, F_2 $(J = N+1/2)$, F_3 $(J = N-1/2)$ and F_4 $(J = N-3/2)$.

With a value of $A/B \sim 47$, the $a^4\Pi_u$ state of O_2^+ is a good Hund's case (a)

state. Ω, the projection of J on the internuclear axis, is a good quantum number in this limit. The fine structure levels are, in order of increasing energy: F_1 (Ω=5/2), F_2 (Ω=3/2), F_3 (Ω=1/2), and F_4 (Ω=$-$1/2). The spin projection quantum number Σ varies from $-3/2$ to $+3/2$. For the F_1 and F_4 levels, $\Sigma = \pm 3/2$, while for the F_2 and F_3 levels, $\Sigma = \pm 1/2$.

As the nuclei rotate faster, the spin uncouples from the internuclear axis, and Σ is no longer a good quantum number. The spin-rotation interaction mixes states of different Σ but the same J and parity. In the limit of large J, the spin becomes completely uncoupled from the nuclear frame; the state is then described by Hund's case (b). The coupling case is intermediate for the $a^4\Pi_u$ state for values of J between about 16.5 and 26.5.

Fig. 7 shows more detailed scans of the Δv=3 sequence taken at 0.1 ms and 100 ms. The band origins for the different vibrational levels fortuitously coincide. At 100 ms, the center of these bands has lost the most intensity. This can be understood if one realizes that each band consists of four sub-bands, which to a first approximation are spaced by the $a^4\Pi_u$ spin-orbit coupling constant $A \approx 50$ cm^{-1}. Each sub-band effectively arises from a different value of Ω. Because the vibrational origins coincide in this sequence, these sub-bands are fairly easily distinguished, despite the spectral congestion. Of course, as the value of J increases, this picture deteriorates, but it is probably a reasonable description of the spectrum with a room temperature rotational distribution. From low photon energy to high, the sub-band ordering is Ω=+5/2, +3/2, 1/2 and $-1/2$. The intensity in the center of the broad envelope arises from absorption by $a^4\Pi_u$ levels F_2 and F_3; thus, we can conclude that the $a^4\Pi_u$ levels F_2 and F_3 decay significantly faster than the F_1 and F_4 levels.

Closer inspection of the spectra reveals line by line differences in the lifetimes, observable even on time scales less than 100 ms. The low resolution of the experiment has made it difficult to assign individual lines; most lines were blended. We chose to look at the decays of two unidentified lines in the Δv=3 sequence, one at 4947.0 Å from the faster decaying center and one at 4967.2 Å from the slower decaying region. These decays are shown in Fig. 5.

While the decay of the signal at the two wavelengths differ, for both, the decay is nonexponential. The decays are complicated by the fact that at any wavelength, one can produce O^+ fragments by direct dissociation to the repulsive states. There are at least two repulsive curves that are accessible.[10,11] Since all initial $a^4\Pi_u$ levels will absorb into the continuum, the continuous part of the signal will exhibit a multiple exponential decay, and is a measure of the decay of the total O_2^+ $a^4\Pi_u$ population. We have followed the decay to 350 ms (the count rate has decayed by 50% from 100 ms), and found that it is still not described by a single exponential.

The observed decay at a given wavelength is the sum of contributions from the continuum spectrum and from the discrete spectrum. To get the decay rate of a discrete line, the continuum contribution must be subtracted. The direct dissociation signal should have a very weak wavelength dependence. By taking the difference between the two decay curves, the wavelength independent background can be eliminated. Fig. 8 is a plot of the difference. The solid line is the curve

$$Y(t) = Y_1 e^{-t/\tau_1} - Y_2 e^{-t/\tau_2} \tag{3}$$

fitted to the data, with τ_1= 130 ms and τ_2= 7 ms. The dotted lines are bounds, from which we obtain the error bars, yielding the following lifetimes: 130 ±50 ms at 4967.2 Å and 7 ±2 ms at 4947.0 Å. Because we did not identify the transitions involved, these values can only be treated as qualitatively representative of the

lifetimes of the spin components.

We have simulated the decay spectra of the Δv=3 sequence,[29] giving the F_1 and F_4 levels a lifetime of 130 ms and the F_2 and F_3 levels a lifetime of 7 ms. The spectra at 0.1 ms and 100 ms are shown in Fig. 9, for comparison with the observed spectra in Fig. 7. At 100 ms, the F_2 and F_3 components are essentially gone, and the simulated spectrum reproduces the large "hole" in the center of the envelope. Of course, this is a very crude simulation, since we have observed that the decay rates vary over a wide range, but it does serve to give a qualitative picture of the spectra at these two times, and support our hypothesis on the fine structure dependence of the decay.

IV. DISCUSSION

We have argued that the lifetimes depend strongly on the spin component of the $a^4\Pi_u$ state. The decay can be qualitatively understood in terms of a unique perturber approximation. Our discussion follows that of James[30] for the spin-forbidden transition $a^3\Pi \rightarrow X^1\Pi$, the Cameron Band, of CO. Spin-orbit coupling mixes pure spin states, allowing a spin-forbidden decay to occur. The true rovibronic eigenstate $|\psi\rangle$ can be expressed as

$$|\psi\rangle = |a^4\Pi_u; F_i\rangle + \sum_j \frac{1}{E_a - E_j} |j\rangle\langle j| H_{SO} |a^4\Pi_u; F_i\rangle \qquad (4)$$

where the $|j\rangle$=$|n\Lambda(S)\Sigma v; JM_J\rangle$ states that are important in this case are doublet states. The $A^2\Pi_u$ state lies only 0.95 eV above the $a^4\Pi_u$ state,[31] and provides the most likely intermediate state responsible for the $a^4\Pi_u \rightarrow X^2\Pi_g$ transition strength. The next nearest ungerade doublet states have not yet been experimentally observed. CI calculations predict a $^2\Pi_u$ state and a repulsive $^2\Sigma_u$ state about 3 eV above the A state.[32] Nuclear inversion symmetry forbids mixing of the a state with

the ground state itself. The $X^2\Pi_g$ states are also given by an expression similar to Eq. 4. Spin-orbit coupling of the $X^2\Pi_g$ state to quartet states will also contribute to the oscillator strength of the $a^4\Pi_u \rightarrow X^2\Pi_g$ transition. The nearest quartet states that can mix with the $X^2\Pi_g$ state are the $b^4\Sigma_g^-$ state, 6 eV above, and dissociative states near the b state. The energy denominator in Eq. 4 decreases the importance of these couplings. In summary, the most important term in the spin-orbit perturbation expansions appears to be coupling of the $a^4\Pi_u$ and $A^2\Pi_u$ states. The $a^4\Pi_u \rightarrow X^2\Pi_g$ transition thus borrows intensity from the allowed $A^2\Pi_u \rightarrow X^2\Pi_g$ transition, the Second Negative Band,[33] which has a lifetime of 1.0 μs.[34,35]

If the $A^2\Pi_u$ is the dominant contribution, we can account for the observed dependence of the decay rate on the fine structure component. The spin-orbit operator in the LS coupling limit can be written as

$$H_{SO} = A\,\mathbf{L}\cdot\mathbf{S} = A(L_zS_z + L_+S_- + L_-S_+) \tag{5}$$

resulting in non-zero off-diagonal matrix elements obeying the selection rules

$$\Delta\Sigma = -\Delta\Lambda = 0, \pm 1 \tag{6}$$

in the Hund's case (a) basis set. For coupling of the a and A states, $\Delta\Lambda$=0; therefore only the Σ=$\pm$1/2 components of the $a^4\Pi_u$ state will mix. The spin-orbit interaction will not mix the Σ=$\pm$3/2 components with the A state. In the Hund's case (a) limit, the F_2 and F_3 levels are predominantly Σ=$\pm$1/2 states, while the F_1 and F_4 levels are predominantly Σ=$\pm$3/2 states. Thus, if we assume that coupling to the $A^2\Pi_u$ state is the largest, the F_1 and F_4 components will couple more weakly and have longer radiative lifetimes.

As J increases, spin-rotation coupling will mix the Σ=$\pm$3/2 with the Σ=$\pm$1/2. The F_1 and F_4 components will have increasingly mixed Σ character and their

lifetimes will therefore decrease for larger values of J. Thus, one expects a J-dependence to the lifetime as well. This would explain the small variations in decay rates we observed in the more detailed scans. Calculations on the spin-forbidden decay of CO ($a^3\Pi$) illustrate such a dependence on the fine structure component and the rotational quantum number. Spin-orbit coupling with other states will also contribute, making more significant contributions to the F_1 and F_4 levels, particularly at lower J, as Fournier *et al.*[36] have shown for the J=0 states in the Cameron band. Kovacs[37] has performed a general analysis for the spin-orbit coupling of a $^4\Pi$ with a $^2\Pi$ state of a diatomic molecule. Those calculations corroborate the qualitative picture presented here. In summary, spin-orbit coupling mixes the F_2 and F_3 levels, with $\Sigma=\pm 1/2$, with the $A^2\Pi_u$ state; thus, these levels decay faster than the F_1 and F_4 levels, which at lower J are predominantly $\Sigma=\pm 3/2$.

Many vibrational states of $a^4\Pi_u$ are also populated, and the radiative lifetimes will also depend on the vibrational quantum number. The variation arises from two effects. First, the spin-orbit matrix element will depend on the vibrational levels of the coupled states. The variation in the matrix elements may be averaged out to some extent, because the perturbation expansion involves a sum over all intermediate vibrational levels, and the radiative lifetime is a sum over transitions to all final vibrational levels. Perhaps more important will be the energy denominator in Eq. 4, because the $A^2\Pi_u$ state lies so close in energy to the $a^4\Pi_u$ state.

O'Keefe and McDonald measure a lifetime of $0.22^{+0.03}_{-0.02}$ s for the $a^4\Pi_u$ state using an ICR trap.[13] In their experiment, the $a^4\Pi_u$ population is probed by reaction with Ar. Thus, the background pressure, greater than 10^{-7}, is relatively high. The O_2^+ parent ions are first allowed to relax for 50 ms prior to the beginning of measurements. All unwanted masses are ejected after the relaxation period. From our

results, it is clear that the F_2 and F_3 levels, as well as states with higher J values, will have radiatively relaxed before O'Keefe and McDonald start their measurements. They measure only the longest-lived fraction of the O_2^+ $a^4\Pi_u$ states, although inelastic scattering may repopulate levels depleted by radiative decay. Their long lifetime is therefore consistent with our results. Any theoretical estimate of the lifetime, averaged over some expected initial distribution of states but neglecting the initial relaxation, should yield lifetimes shorter than 0.22 s. Our observation of a decay dependent upon the spin projection quantum number raises another question: can the magnetic field that traps the ions give rise to Zeeman coupling of the spin components? If so, the lifetime observed in an ICR trap would not be identical to that in field-free space.

Theoreticians can now calculate spin-orbit matrix elements with accurate, correlated wavefunctions, and have calculated radiative decay rates for spin-forbidden transitions in simple molecules.[38] There have been several configuration interaction (CI) calculations[32,39] of the low lying excited states of O_2^+, as well as reports of CI level *ab initio* spin-orbit matrix elements. Carre *et al.*[41] have calculated the spin-orbit coupling of the $b^4\Sigma_g^-$ state to neighboring repulsive states to determine the mechanism for predissociation of the b state. Brown *et al.*[42] report a reduced matrix element $\langle a^4\Pi_u \| H_{SO} \| A^2\Pi_u \rangle$ used to estimate third-order perturbation terms for the First Negative band within the unique perturber approximation. Finally, Marian *et al.*[32] have performed a large scale MRD-CI calculation of O_2^+. In that work, they have calculated the perturbation term by summing over several low-lying states of O_2^+, rather than using a single perturbing state. With this approach, they have calculated the spin-orbit induced predissociation rate of the $b^4\Sigma_g^-$ state, as well as the spin-orbit splitting in the $X^2\Pi_g$ state. The calculation of the radiative lifetimes

of the rovibronic levels of the $a^4\Pi_u$ state should be a straightforward application of the wavefunctions and methods used by these authors.

For the best comparison of experiment and theory, lifetimes of individual states are needed. In principle, this apparatus is capable of such measurements, but in the current experiment the spectral resolution limits our ability to obtain more quantitative results. Thus, we have been able only to demonstrate the qualitative features of the radiative decay of the $a^4\Pi_u$ state. To measure the dependence of the radiative lifetime on both the fine structure component and on J, we must narrow the resolution and/or decrease congestion by cooling the rotations or vibrations.

ACKNOWLEDGMENTS

This work was supported by the Director, Office of Energy Research, Office of Basic Energy Sciences, Chemical Sciences Division of the Department of Energy under Contract No. DE-AC03-76SF00098. D.G. acknowledges financial support from the Deutsche Forschungsgemeinschaft, and M.O. acknowledges the support of a General Electric Fellowship.

REFERENCES

1. A. Dalgarno and M. B. McElroy, Planet. Space Sci. **13**, 947 (1965).

2. E. E. Ferguson, F. C. Fehsenfeld, and D. L. Albritton, in *Gas Phase Ion Chemistry* (edited by M. T. Bowers), 45 (Academic Press, New York, 1979).

3. P. H. Krupenie, J. Phys. Chem. Ref. Data **1**, 423 (1972).

4. T. O. Tiernan and C. Lifschitz, Adv. Chem. Phys. **45**, 81 (1981); K. Tanaka, T. Kato, P. M. Guyon, and I. Koyano, J. Chem. Phys. **77**, 4441 (1982) ; *ibid.* **79**, 4302 (1983); P. H. Dawson, Int. J. Mass Spectrom. Ion Phys. **63**, 305 (1985).

5. T. E. Nevin, Phil. Trans. R. Soc. London Ser. A **237**, 471 (1938); Proc. R. Soc. London Ser. A **174**, 371 (1940); T. E. Nevin and T. Murphy, Proc. R. Ir. Acad. Sect. A **46**, 169 (1941); D. L. Albritton, A. L. Schemltekopf, W. J. Harrop, R. N. Zare, and J. Czarny, J. Mol. Spectrosc. **67**, 157 (1977).

6. M. L. Vestal, G. Mauclaire, and F. H. Futrell, in *23rd Annu. Conference on Mass Spectrom.*(Houston, Texas, 1975).

7. J. T. Moseley, M. Tadjeddine, T. Durup, J. B. Ozenne, and J. Durup, Phys. Rev. Lett. **37**, 891 (1976).

8. A. Carrington, P. G. Roberts, and P. J. Sarre, Mol. Phys. **34**, 291 (1977) ; *ibid.* **35**, 1523(1978).

9. J. C. Hansen, J. T. Moseley, and P. C. Cosby, J. Mol. Spectrosc. **98**, 48 (1983).

10. J. T. Moseley and J. Durup, Annu. Rev. Phys. Chem. **32**, 53 (1981).

11. J. T. Moseley, Adv. Chem. Phys. **60**, 245 (1985).

12. D. W. Vance, Phys. Rev. **169**, 263 (1968).

13. A. O'Keefe and J. R. McDonald, Chem. Phys. **103**, 425 (1986).

14. R. Schneider and G. Werth, Z. Phys. **A293**, 103 (1979); R. D. Knight and M. H. Prior, Phys. Rev. **A21**, 179 (1980); F. Plumelle, M. DeSaintfuschien, J. L. Duchene, and C. Audoin, Opt. Commun. **34**, 71 (1980); A. Osipowicz and G. Werth, Opt. Commun. **36**, 359 (1981); J. C. Bergquist, D. J. Wineland, W. M. Itano, H. Hemmati, H.-U. Daniel, and G. Leuchs, Phys. Rev. Lett. **55**, 1567 (1985).

15. R. D. Knight, Phys. Rev. Lett. **48**, 792 (1982).

16. C. C. Martner, J. Pfaff, N. H. Rosenbaum, A. O'Keefe, and R. J. Saykally, J. Chem. Phys. **78**, 7073 (1983) And references therein.

17. J. Danon, G. Mauclaire, T. R. Govers, and R. Marx, J. Chem. Phys. **76**, 1255 (1982).

18. H. G. Dehmelt, Adv. At. Mol. Phys. **3**, 53 (1967) ; *ibid.* **5**, 109 (1969).

19. D. J. Wineland, W. M. Itano, and R. S. van Dyck, Adv. At. Mol. Phys. **19**, 135 (1983).

20. L. D. Landau and E. Lifschitz, *Mechanics* (Pergamon Press, Oxford, 1960).

21. E. Teloy and D. Gehrlich, Chem. Phys. **4**, 417 (1974).

22. D. Gehrlich, in *Electronic and Atomic Collisions* (edited by D. C.Lorents, W. E. Meyerhof, and J. R. Peterson), 451 (North-Holland, Amsterdam, 1985).

23. K. M. Ervin and P. B. Armentrout, J. Chem. Phys. **83**, 166 (1985).

24. P. H. Dawson and J. E. Fulford, Int. J. Mass Spectrom. Ion Phys. **42**, 195 (1982).

25. B. R. Turner, J. A. Rutherford, and D. M. J. Compton, J. Chem. Phys. **48**, 1602 (1968).

26. H. A. Enge, Rev. Sci. Instrum. **30**, 248 (1959); C. F. Giese, Rev. Sci. Instrum. **30**, 260 (1959); C. S. Lu and H. E. Carr, Rev. Sci. Instrum. **33**, 823 (1962); M. L. Vestal, PhD thesis, University of Utah, Utah, 1975.

27. H. D. Zeman, Rev. Sci. Instrum. **48**, 1079 (1977).

28. R. N. Daly, Rev. Sci. Instrum. **31**, 264 (1960).

29. R. Frey, R. Katoschke, K. Muller-Dethlefs, and E. W. Schlag, Z. Phys. **A307**, 25 (1982).

30. T. C. James, J. Chem. Phys. **55**, 4118 (1971).

31. K. P. Huber and G. Herzberg, *Molecular Spectra and Molecular Structure: IV. Constants of Diatomic Molecules* (van Nostrand Reinhold, New York, 1979).

32. C. M. Marian, R. Marian, S. D. Peyerimhoff, B. A. Hess, R. J. Buenker, and G. Seger, Mol. Phys. **46**, 779 (1982).

33. J. A. Coxon and M. P. Haley, J. Mol. Spectrosc. **108**, 119 (1984).

34. M. Jeunehomme, J. Chem. Phys. **44**, 4253 (1966).

35. E. H. Fink and K. H. Welge, Z. Naturforsch. A **23**, 358 (1968); P. Erman and M. Larson, Phys. Scrip. **15**, 3345 (1977).

36. J. Fournier, H. H. Mohammed, J. Deson, C. Vermeil, and J. Schamps, J. Chem. Phys. **73**, 6039 (1980).

37. I. Kovacs, Can. J. Phys. **36**, 309 (1958) ; *ibid.* 329.

38. See for example F. Grein, S. D. Peyerimhoff, and R. J. Buenker, Can. J. Phys. **62**, 1928 (1984); R. Klotz, C. M. Marian, S. D. Peyerimhoff, B. A. Hess, and R. J. Buenker, Chem. Phys. **89**, 223 (1984); R. Klotz and S. D. Peyerimhoff, Mol. Phys. **57**, 573 (1986).

39. N. H. F. Beebe, E. W. Thulstrup, and A. Andersen, J. Chem. Phys. **74**, 2195 (1976); N. Honjou, K. Tanaka, K. Ohno, and H. Taketa, Mol. Phys. **35**, 1569 (1978);

40. P. J. A. Ruttink and J. H. van Lenthe, J. Chem. Phys. **74**, 5785 (1981).

41. M. Carre, M. Druetta, M. L. Gaillard, H. H. Bukow, M. Horani, A. L. Roche, and M. Velghe, Mol. Phys. **40**, 1453 (1980).

42. J. M. Brown, D. J. Milton, J. K. G. Watson, R. N. Zare, D. L. Albritton, M. Horani, and J. Rostas, J. Mol. Spectrosc. **90**, 139 (1981).

FIGURE CAPTIONS

FIG. 1 Potential energy curves of some relevant low lying states of O_2^+. The repulsive $d^4\Sigma_g^-$ state, not shown, also crosses the $b^4\Sigma_g^-$ state near the intersection of the b and f states.

FIG. 2 Schematic of the ion photodissociation spectrometer. The ions are formed by electron impact ionization, mass selected by the sector magnet, and trapped in the rf octopole ion trap. After photolysis with a pulsed dye laser, the products are mass analyzed with a quadrupole mass spectrometer.

FIG. 3 Observed decay, as a function of trapping time, of O_2^+ parent ions(laser off) and of O^+ photofragment signal at two wavelengths, 4967.2 Å and 4947.0 Å.

FIG. 4 Low resolution photodissociation spectrum of O_2^+ $a^4\Pi_u$ at trapping times of 0.1 ms and 100 ms, with a constant baseline subtracted to remove signal from the direct dissociation. The two peaks are band sequences of the First Negative Band $b^4\Sigma_g^- \leftarrow a^4\Pi_u$.

FIG. 5 Decay of O^+ photofragment signal at 4967.2 Å and 4947.0 Å, normalized for loss of parent ions.

FIG. 6 The power dependence of the photodissociation signal for $O_2^+ \rightarrow O^+ + O$ at 5320 Å.

FIG. 7 Photodissociation spectrum of the Δv=3 band sequence of the First Negative Band, at higher resolution than Fig. 4, taken at trapping times of 0.1 ms and 100 ms, again with a constant baseline subtracted.

FIG. 8 Plot of the difference between the two O^+ decay curves (photdissociating wavelengths of 4967.2 Å and 4947.0 Å) shown in Fig. 5. The solid curve is

a fit yielding lifetimes of 7 ms and 130 ms. The dashed curves are estimates of the uncertainty in the fit, with lifetimes of 5 ms and 180 ms for the upper curve and 9 ms and 80 ms for the lower curve.

FIG. 9 Simulation of the photodissociation spectrum of the $\Delta v=3$ band sequence at trapping times of 0.1 ms and 100 ms. The F_1 and F_4 sublevels of the $a^4\Pi_u$ state have a lifetime of 130 ms, while the F_2 and F_3 sublevels have a lifetime of 7 ms.

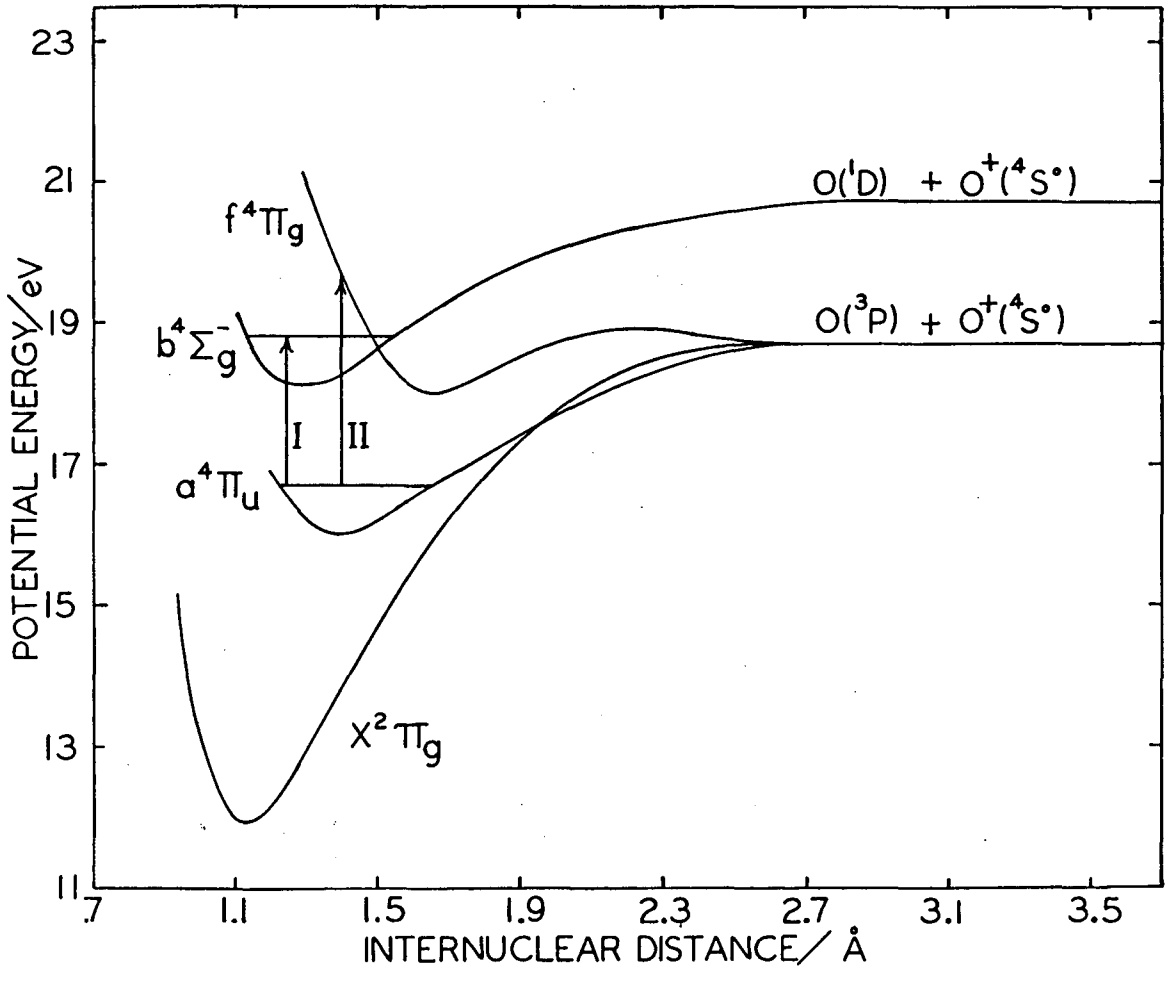

XBL 7812-13896

Figure 1

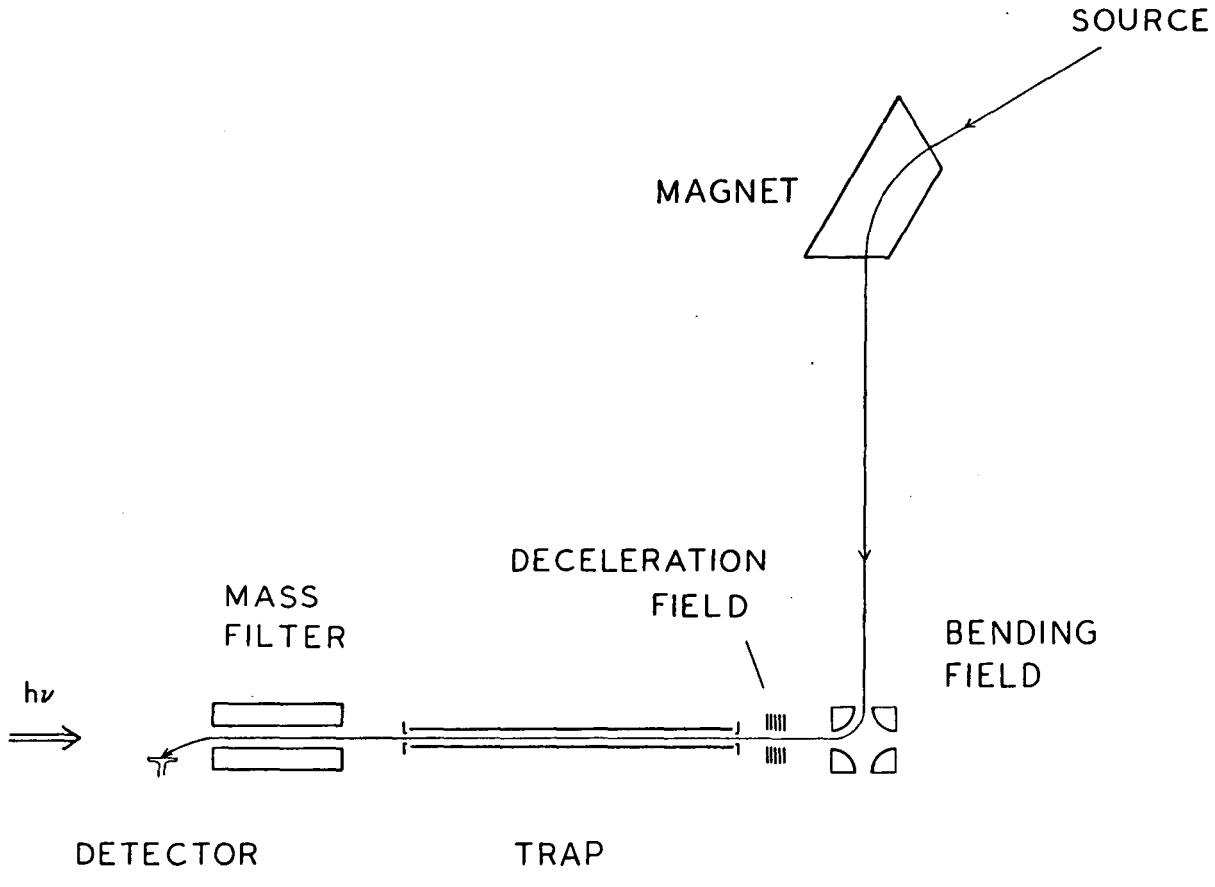

XBL 847-3011

Figure 2

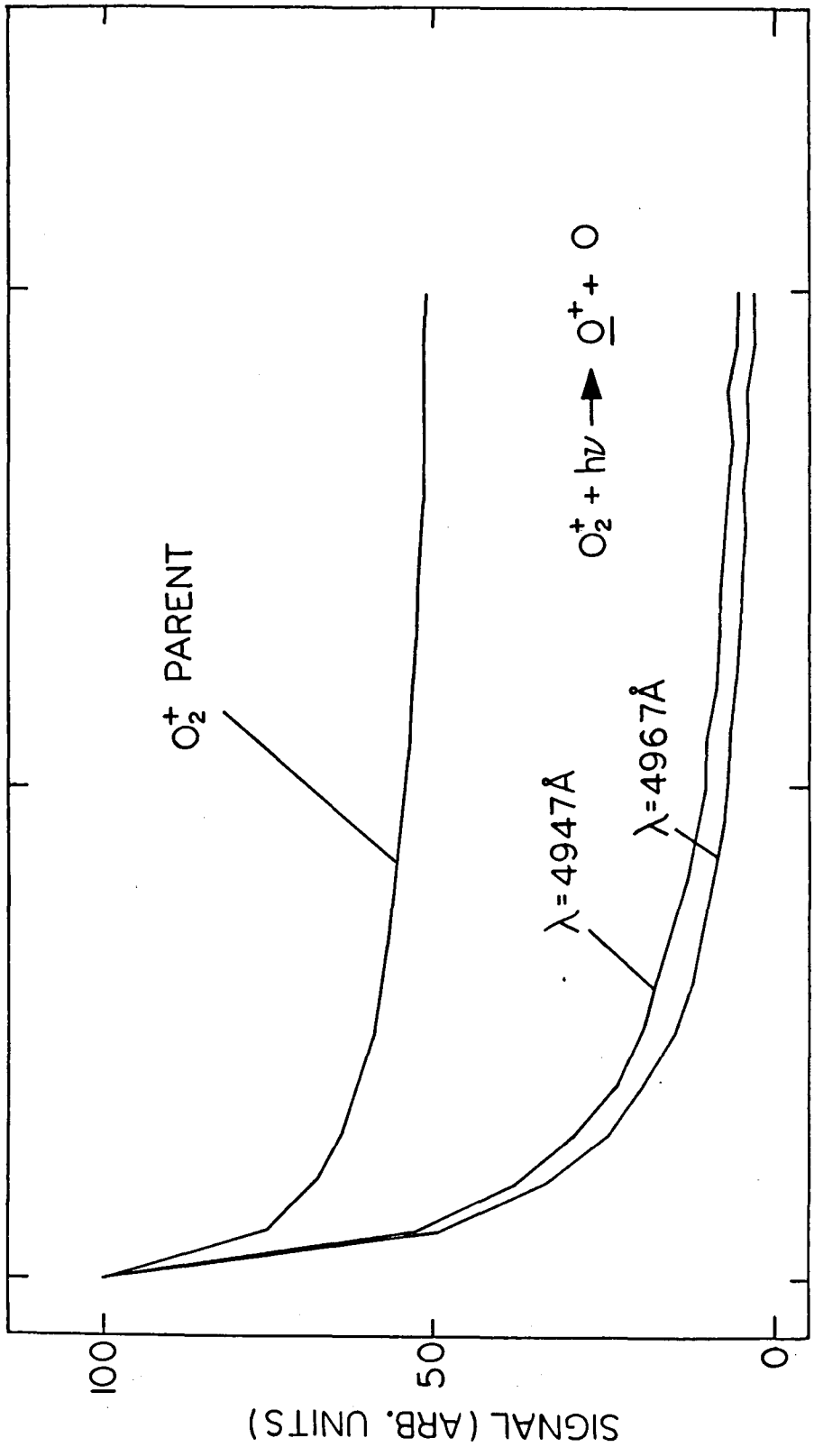

XBL 8311-4415

Figure 3

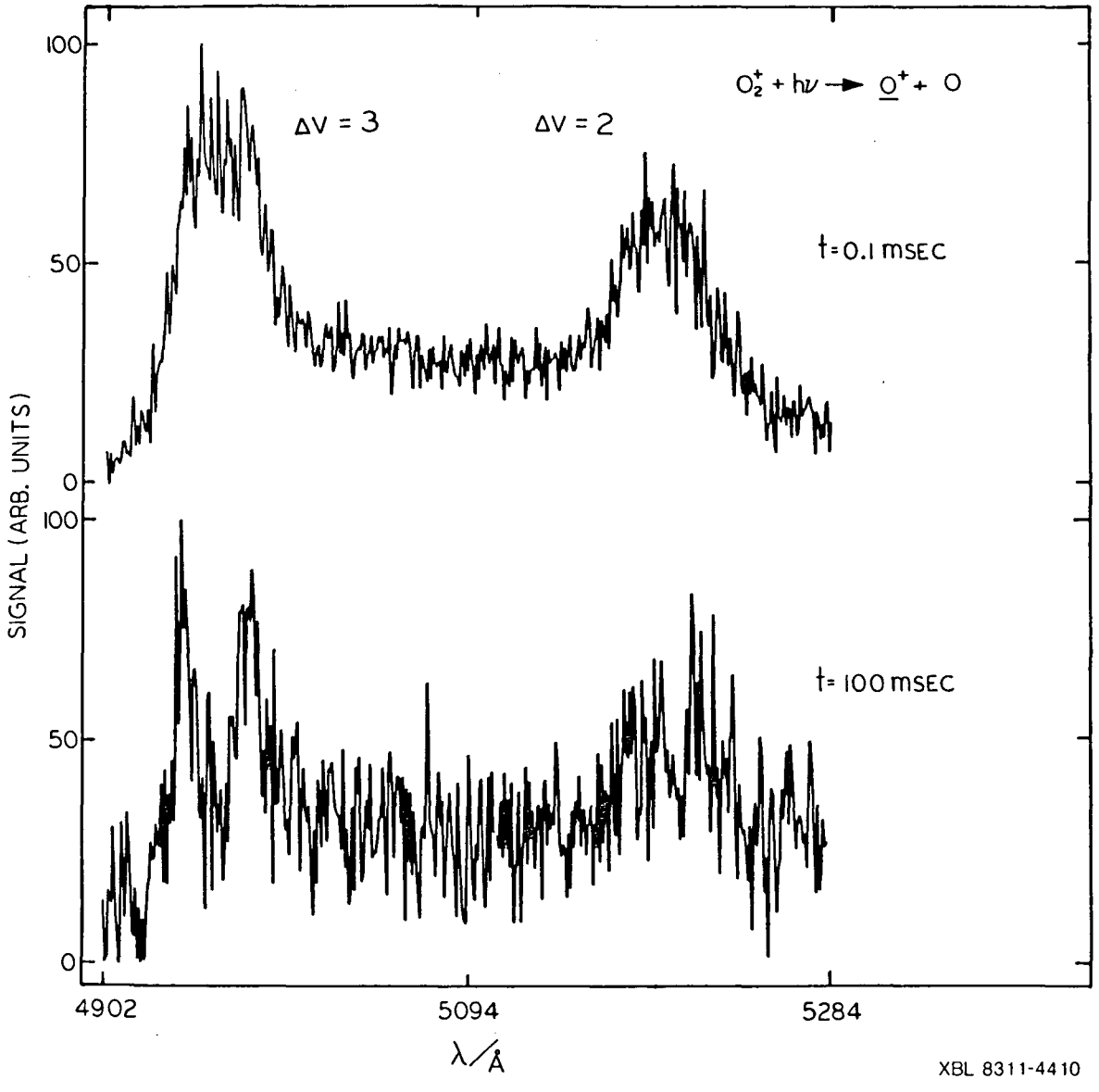
100
50
0
100
50
0
SIGNAL (ARB. UNITS)
$O_2^+ + h\nu \rightarrow \underline{O}^+ + O$
ΔV = 3
ΔV = 2
t = 0.1 msec
t = 100 msec
4902
5094
5284
λ/Å
XBL 8311-4410

Figure 4

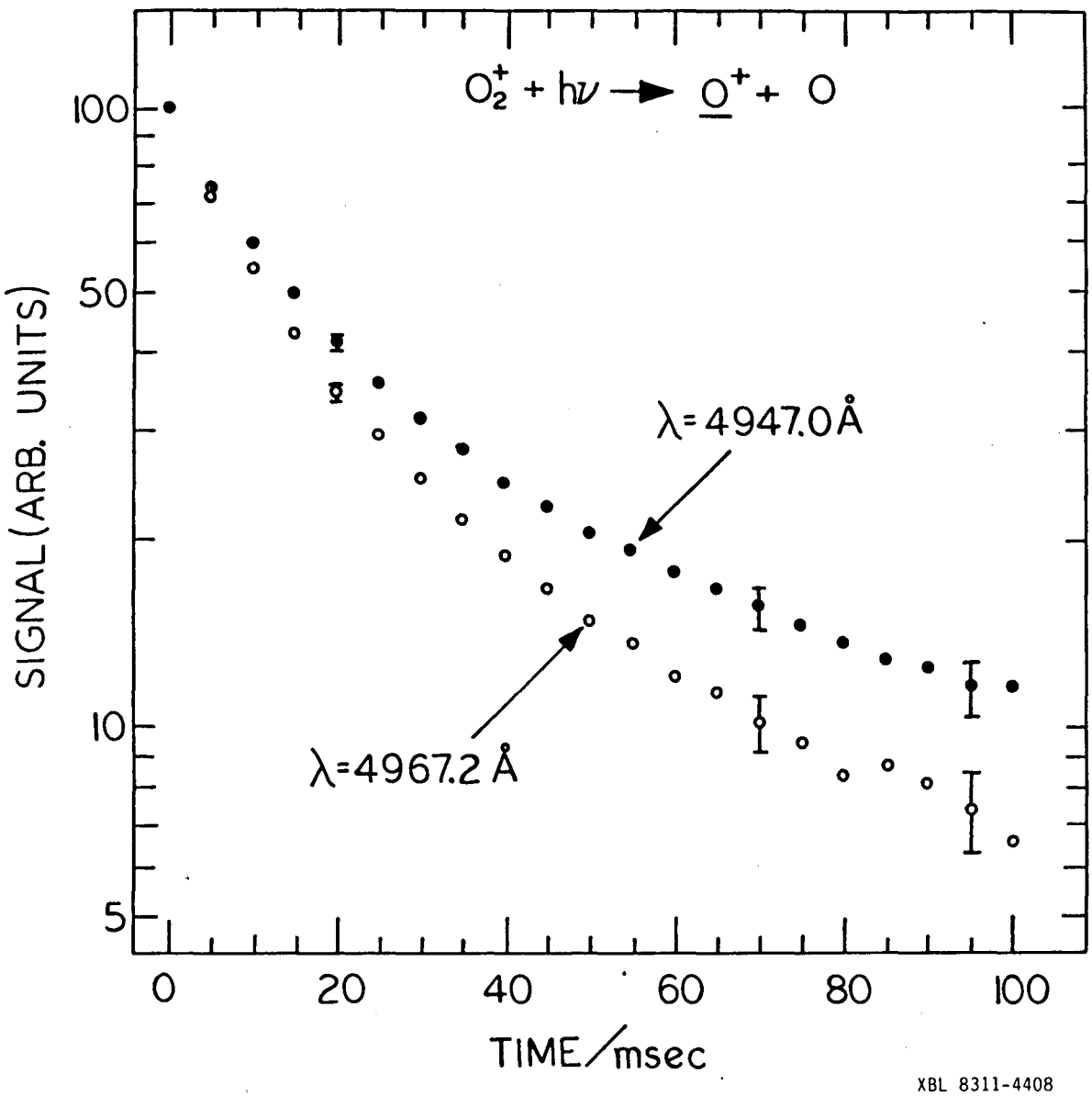
$O_2^+ + h\nu \rightarrow \underline{O}^+ + O$
λ=4947.0Å
λ=4967.2 Å
SIGNAL (ARB. UNITS)
100
50
10
5
0
20
40
60
80
100
TIME/msec
XBL 8311-4408

Figure 5

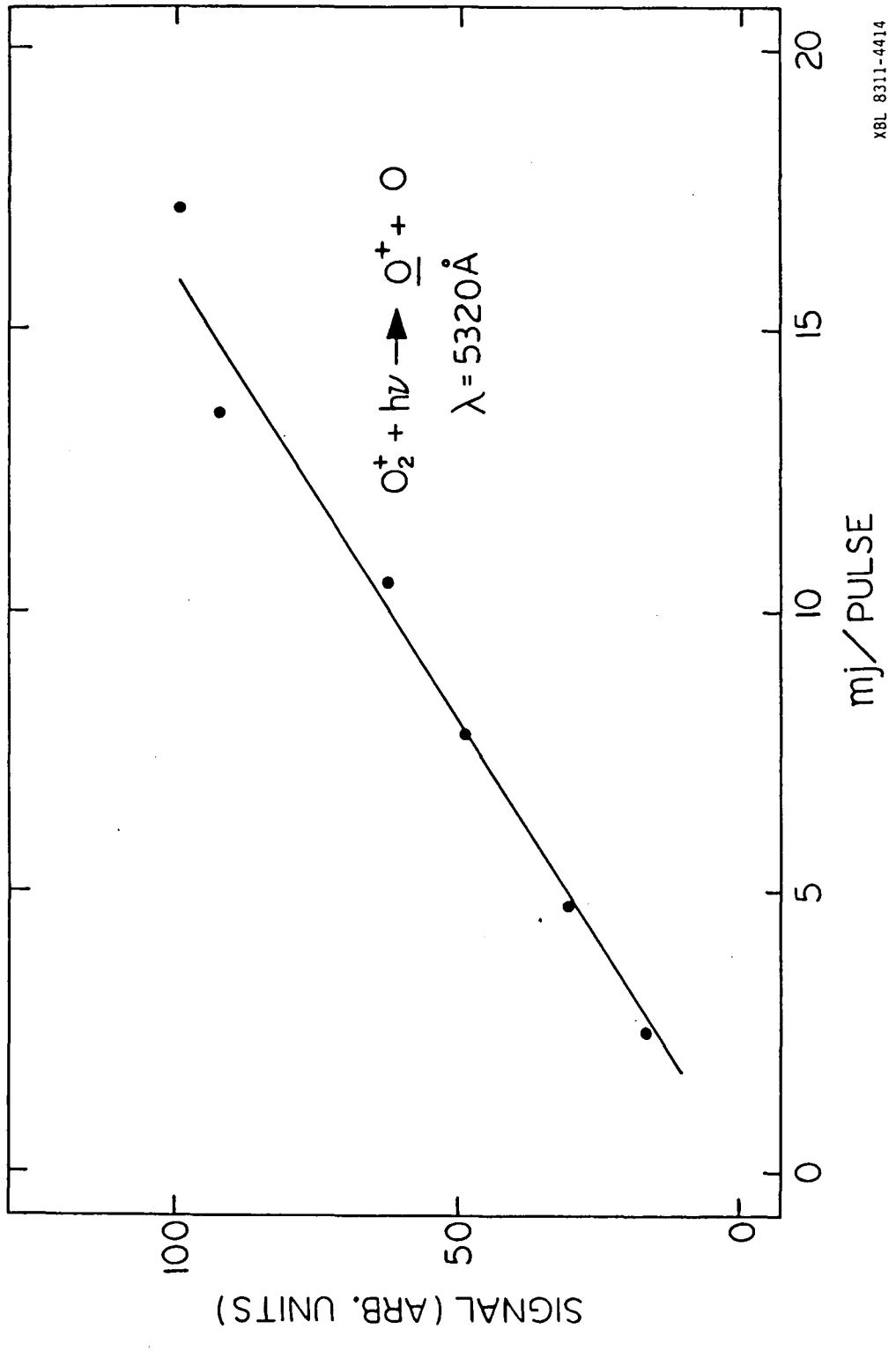
SIGNAL (ARB. UNITS)
0
50
100
0
5
10
15
20
mj/PULSE
$O_2^+ + h\nu \rightarrow O^+ + O$
$\lambda = 5320\text{Å}$
XBL 8311-4414

Figure 6

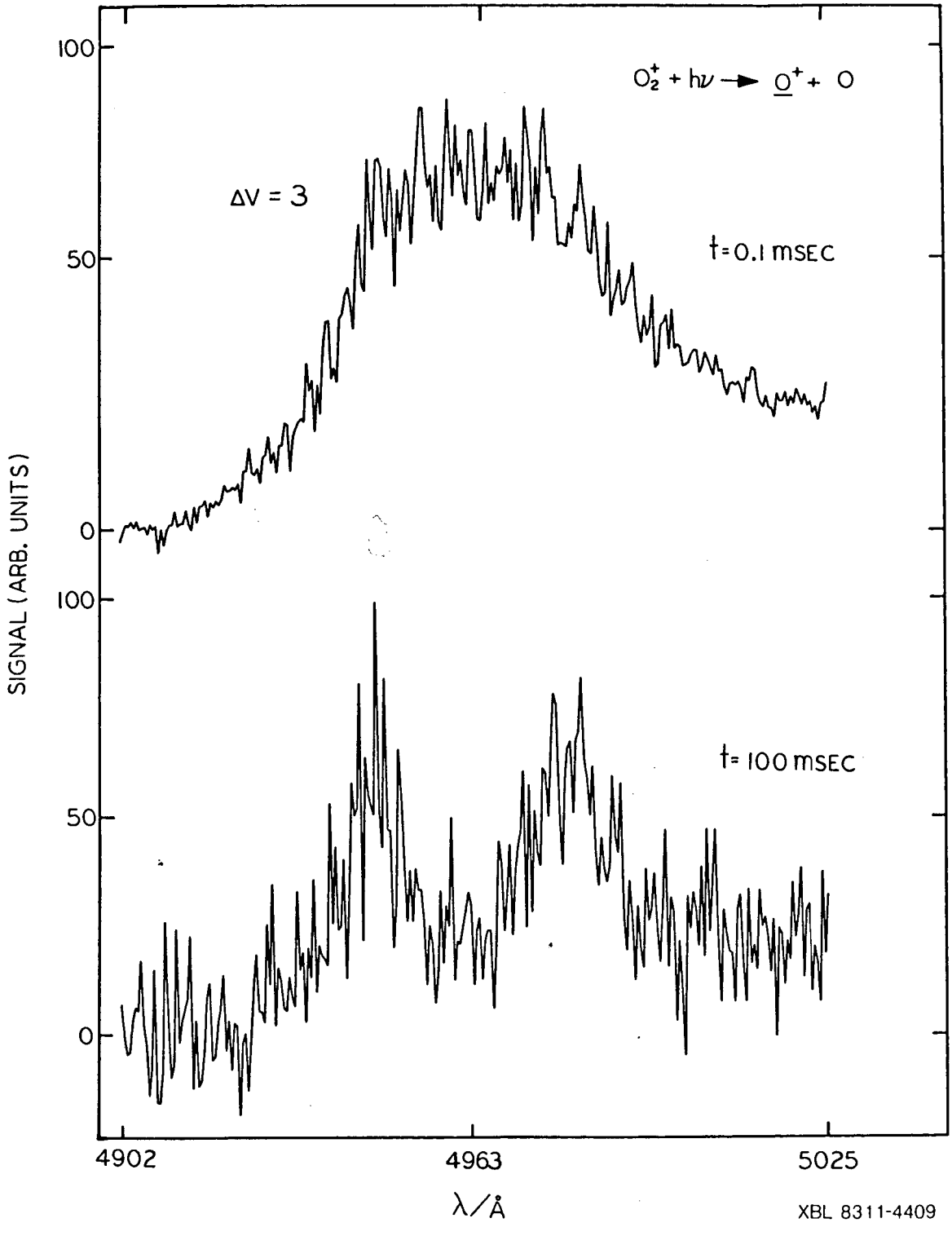
$O_2^+ + h\nu \rightarrow \underline{O}^+ + O$
ΔV = 3
t=0.1 mSEC
t= 100 mSEC
SIGNAL (ARB. UNITS)
100
50
0
100
50
0
4902
4963
5025
λ/Å
XBL 8311-4409

Figure 7

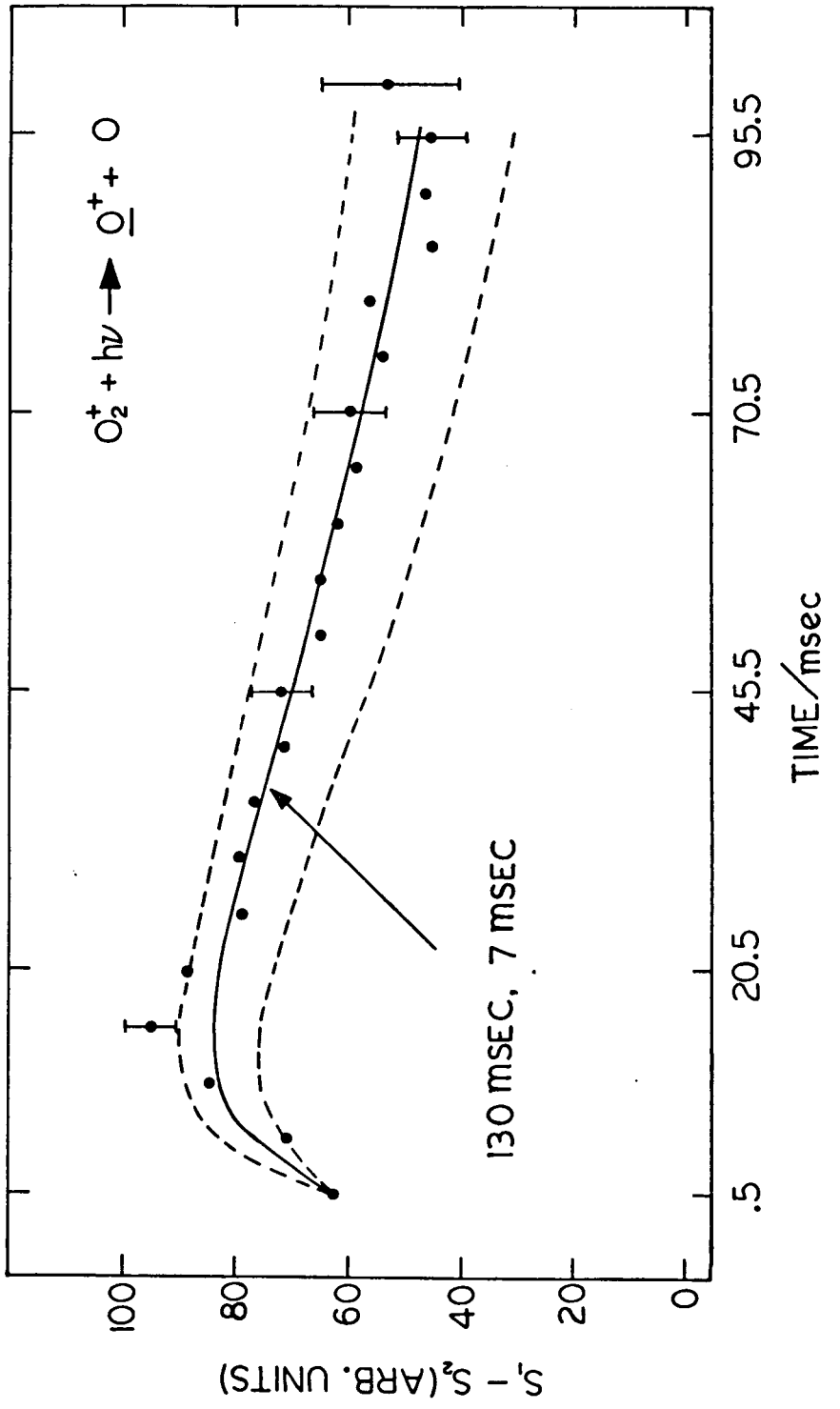

XBL 8311-4469

Figure 8

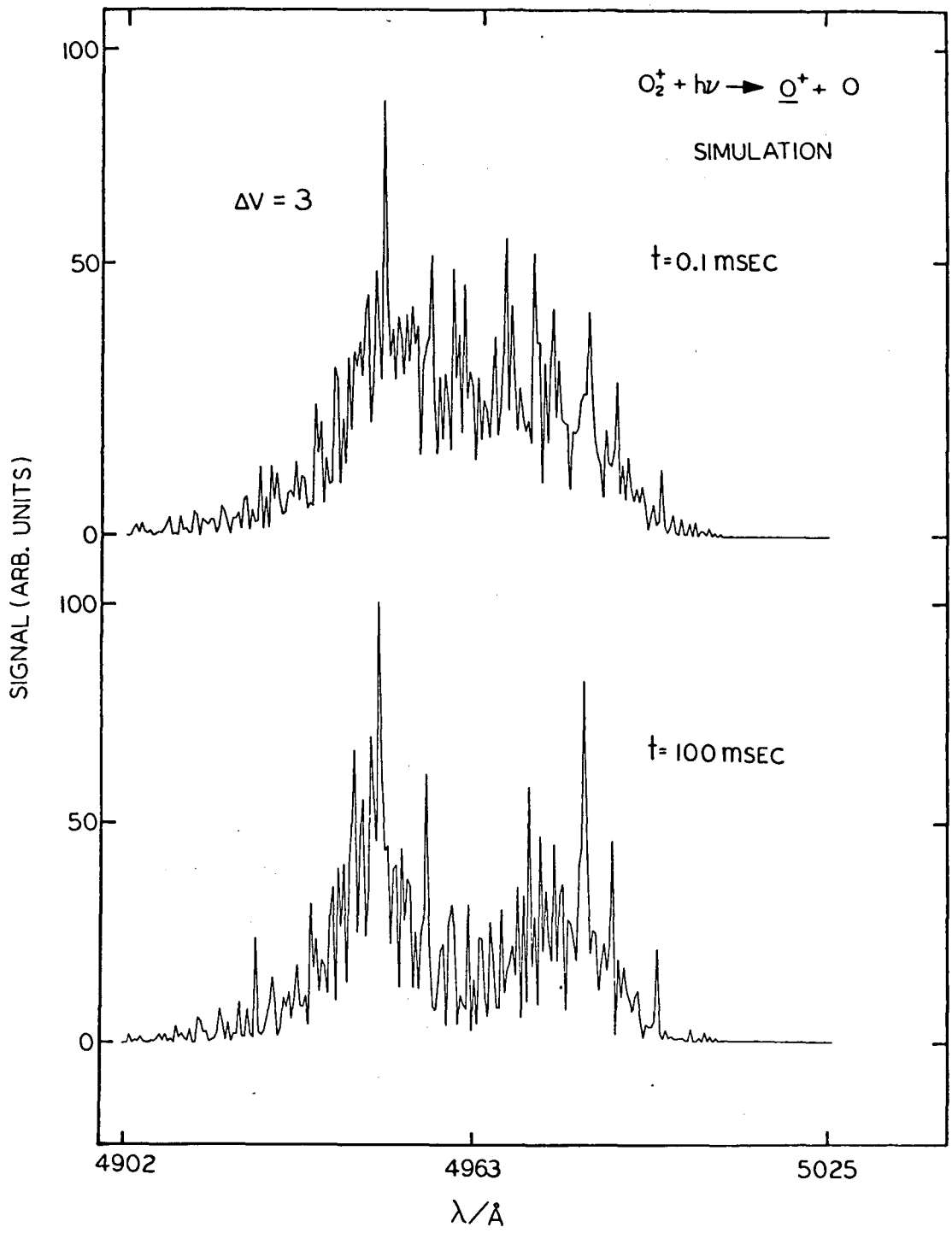

XBL 8311-4470

Figure 9

LAWRENCE BERKELEY LABORATORY
TECHNICAL INFORMATION DEPARTMENT
UNIVERSITY OF CALIFORNIA
BERKELEY, CALIFORNIA 94720